

RESEARCH

Open Access



The role of heparan sulfate in enhancing the chemotherapeutic response in triple-negative breast cancer

Jasmine M. Manouchehri¹, Jharna Datta¹, Lynn M. Marcho¹, Jesse J. Reardon², Daniel Stover¹, Robert Wesolowski¹, Uma Borate³, Ting-Yuan David Cheng⁴, Patrick M. Schnell⁵, Bhuvanewari Ramaswamy¹, Gina M. Sizemore², Mark P. Rubinstein¹ and Mathew A. Cherian^{1,6*}

Abstract

Background Breast cancer, one of the most common forms of cancer, is associated with the highest cancer-related mortality among women worldwide. In comparison to other types of breast cancer, patients diagnosed with the triple-negative breast cancer (TNBC) subtype have the worst outcome because current therapies do not produce long-lasting responses. Hence, innovative therapies that produce persisting responses are a critical need. We previously discovered that hyperactivating purinergic receptors (P2RXs) by increasing extracellular adenosine triphosphate (eATP) concentrations enhances TNBC cell lines' response to chemotherapy. Heparan sulfate inhibits multiple extracellular ATPases, so it is a molecule of interest in this regard. In turn, heparanase degrades polysulfated polysaccharide heparan sulfate. Importantly, previous work suggests that breast cancer and other cancers express heparanase at high levels. Hence, as heparan sulfate can inhibit extracellular ATPases to facilitate eATP accumulation, it may intensify responses to chemotherapy. We postulated that heparanase inhibitors would exacerbate chemotherapy-induced decreases in TNBC cell viability by increasing heparan sulfate in the cellular microenvironment and hence, augmenting eATP.

Methods We treated TNBC cell lines MDA-MB 231, Hs 578t, and MDA-MB 468 and non-tumorigenic immortal mammary epithelial MCF-10A cells with paclitaxel (cytotoxic chemotherapeutic) with or without the heparanase inhibitor OGT 2115 and/or supplemental heparan sulfate. We evaluated cell viability and the release of eATP. Also, we compared the expression of heparanase protein in cell lines and tissues by immunoblot and immunohistochemistry, respectively. In addition, we examined breast-cancer-initiating cell populations using tumorsphere formation efficiency assays on treated cells.

An abstract of this work was previously presented at the American Association for Cancer Research (AACR) Annual Meeting (2023).

*Correspondence:
Mathew A. Cherian
mathew.cherian@osumc.edu

Full list of author information is available at the end of the article



© The Author(s) 2024. **Open Access** This article is licensed under a Creative Commons Attribution-NonCommercial-NoDerivatives 4.0 International License, which permits any non-commercial use, sharing, distribution and reproduction in any medium or format, as long as you give appropriate credit to the original author(s) and the source, provide a link to the Creative Commons licence, and indicate if you modified the licensed material. You do not have permission under this licence to share adapted material derived from this article or parts of it. The images or other third party material in this article are included in the article's Creative Commons licence, unless indicated otherwise in a credit line to the material. If material is not included in the article's Creative Commons licence and your intended use is not permitted by statutory regulation or exceeds the permitted use, you will need to obtain permission directly from the copyright holder. To view a copy of this licence, visit <http://creativecommons.org/licenses/by-nc-nd/4.0/>.

Results We found that combining heparanase inhibitor OGT 2115 with chemotherapy decreased TNBC cell viability and tumorsphere formation through increases in eATP and activation of purinergic receptors as compared to TNBC cells treated with single-agent paclitaxel.

Conclusion Our data shows that by preventing heparan sulfate breakdown, heparanase inhibitors make TNBC cells more susceptible to chemotherapy by enhancing eATP concentrations.

Keywords ATP, Chemotherapy, Heparanase, Purinergic signaling, Breast cancer, Heparan sulfate

Background

Breast cancer has the highest global incidence rate of all cancers with 47.8 new cases and 13.6 deaths per 100,000 per year [1]. Hence, millions of women are affected by breast cancer each year. Moreover, it was the most common cause of cancer-related mortality among women in 2020. Currently, there are few specific targeted therapies, leading to a worse outlook for those patients diagnosed with triple-negative breast cancer (TNBC) as compared to other breast cancer subtypes because of the need for progressively more intrusive and toxic therapies to maintain disease control [2–4]. Thus, the development of more efficacious therapies is needed.

Under physiological conditions, the concentration of intracellular ATP can be between 3 and 10 millimolar (mM), whereas the concentration of eATP is between 0 and 10 nanomolar (nM), a 10^6 -fold difference [5]. Nevertheless, this minute concentration of eATP can act as a signaling molecule through cell surface purinergic receptors [6–8]. Notably, there is a significant difference in extracellular adenosine triphosphate (eATP) concentrations between cancers and normal tissues [6–8]. Our previously published study demonstrated that eATP is toxic (in the high micromolar range) to TNBC cells, but not to nontumorigenic immortal mammary epithelial MCF-10A cells [9]. However, eATP can be broken down by different ecto-nucleotidases, including ecto-nucleoside triphosphate diphosphohydrolases (ENTPDases), 5′nucleotidases (5′-NTs), ecto-nucleotide pyrophosphatases/phosphodiesterases (E-NPPases), and tissue non-specific alkaline phosphatases (TNAP). E-NTPDases are considered the principal enzymes responsible for ATP degradation with extracellular 5′NT responsible for the catalytic conversion of adenosine monophosphate (AMP) to adenosine [10]. We previously showed that inhibitors of each of these families of ecto-ATPases possess the capacity to enhance concentrations of eATP released by cancer cells through P2RX4 and P2RX7 ion channel-coupled purinergic receptors [9]. Thus, attenuation of the activity of all ectoATPases may be necessary to maximize eATP release and TNBC cell death. The presence of multiple families of ecto-ATPase inhibitors complicates the design of synthetic inhibitors. As part of our interest in broad-spectrum ecto-ATPase inhibitors, our appraisal of the literature revealed that polysulfated

polymers such as heparan sulfate (HS) inhibit multiple classes of ecto-ATPases [11, 12]. Hence, we hypothesized that enhancement of extracellular heparan sulfate levels would exacerbate chemotherapy-induced eATP release and TNBC cell death.

The polysulfated polysaccharide heparan sulfate is synthesized in the Golgi system and is composed of disaccharide units that are negatively charged and unbranched, with sulfation on 3-O, 6-O, or N sites of glucosamine as well as the 6-O site on glucuronic/ido-uronic acid [13–16]. Heparan sulfate impacts growth factor signaling, regulates cell adhesion, and sequesters growth factors in the extracellular matrix (ECM) [14, 15, 17]. Heparan sulfate proteoglycans also modulate signaling by the hedgehog, the epidermal growth factor/EGF, fibroblast growth factor (FGF) and vascular endothelial growth factor (VEGF) pathways [18–20]. Heparan sulfate also modulates inflammatory processes by limiting the diffusion of cytokines/chemokines from the immediate pericellular microenvironment and promoting the initiation of innate immune responses [15, 17]. Hence, heparan sulfate may also exert its effects through mechanisms independent of eATP.

Heparanase, the enzyme that degrades heparan sulfate, localizes in the nucleus, lysosomes, and late endosomes; elevated levels of this enzyme have been observed in a variety of cancers, including breast cancer [13–16, 21, 22]. Heparanase can confer chemotherapeutic resistance in cancer cells through numerous mechanisms including autophagy and nuclear factor-kappa B (NF-κB) signaling [23, 24]. Importantly, the growth of tumor xenografts is inhibited by siRNA-mediated heparanase depletion, supporting a protumorigenic role for this enzyme [15].

Various heparanase inhibitors have been developed previously, including neutralizing antibodies, peptides, and small molecules, such as OGT 2115, suramin, PI-88, SST0001, M402, and PG545. These have revealed some effectiveness in vitro and in vivo. OGT 2115 has been tested in prostate cancers and shown to have proapoptotic effects, but was not tested in triple-negative breast cancer; PI-88 has been utilized in phase II clinical trials related to prostate cancer while SST0001 has been used in phase I/II clinical trials for multiple myeloma [13–16, 25–28]. We postulated that heparanase inhibitors would sensitize TNBC cells to chemotherapy by increasing

heparan sulfate in the cellular microenvironment, thus enhancing the concentration of eATP. Therefore, heparanase inhibition is a potential therapeutic strategy for TNBC.

Methods

Cell culture and drugs and chemicals

Breast cancer cell lines MDA-MB 231 (ATCC HTB-26, RRID: CVCL_0062), MDA-MB 468 (ATCC HTB-132, RRID: CVCL_0419), and Hs 578t cells (ATCC HTB-126, RRID: CVCL_0332), and HEK-293T cells (ATCC Cat# CRL-3216, RRID: CVCL_0063) were maintained in DMEM (Corning; Cat#MT10013CV) and supplemented with 10% FBS (Gibco; Cat# A5256801), 1% MEM non-essential amino acids (Gibco; Cat# 11140050), 1 mM sodium pyruvate (Gibco; 11360070), 4 mM Glutamax (Gibco; Cat#35050061) and antimicrobial agents (100 units/ml Penicillin, 100 µg/ml streptomycin, and 0.25 µg/ml amphotericin B) (Gibco; Cat# 15140122). Non-tumorigenic immortalized mammary epithelial MCF-10A cells (ATCC Cat# CRL-10317, RRID: CVCL_0598) were maintained in DMEM/F12 (Gibco; Cat# 11320082) supplemented with 5% horse serum (Gibco; Cat# 26050088), hydrocortisone (Sigma; Cat# H0888-1G), epidermal growth factor (Sigma; Cat# SRP3027), cholera toxin (Sigma; Cat# C8052), insulin (Sigma; Cat# 91077 C) and antimicrobial agents. The cell lines were authenticated and maintained at 37 C, 5% CO₂ and 95% relative humidity as described previously [9].

The following drugs and chemicals were used: ATP (Sigma), recombinant heparanase (Sigma), paclitaxel (Calbiochem), OGT 2115 (Tocris), A438079 (Tocris), 5-BDBD (Tocris), and heparan sodium sulfate (Sigma). Heparan sulfate and ATP were dissolved in nuclease-free water (Invitrogen); paclitaxel, OGT 2115, A438079, and 5-BDBD were dissolved in dimethyl sulfoxide (DMSO) (Sigma). Table 1 shows the drugs' concentrations and functions; we optimized the drug concentrations that were used for the different assays, starting with the previously used drug concentrations as starting points [28–32]. Drugs were added to media at designated concentrations and applied to cells in culture.

Table 1 Drug concentrations and functions

Drug	Concentration(s)	Function(s)	Concentration reference
Paclitaxel	50 and 100 µM	Chemotherapeutic agent	[29]
OGT 2115	20 µM	Heparanase inhibitor	[28]
A437809	20 µM	P2RX7 inhibitor	[30]
5-BDBD	20 µM	P2RX4 inhibitor	[31]
Heparan sodium sulfate	50 µM	developmental processes, angiogenesis, and tumor metastasis	[32]

ELISAs

TNBC and MCF-10A cells were grown for 48 h and supernatants were collected. The basal expression levels of heparanase (Abcam, Cat# ab256401) and heparan sulfate (Lifespan Biosciences, Cat# LS-F22183) were assessed in the examined cell lines via enzyme-linked immunoassay (ELISA) analysis according to the corresponding manufacturer's directions.

Immunohistochemistry of heparanase

AMSBIO BR1202B breast cancer tissue array (120-core array with 82 TNBC cores) on Fisher Superfrost Plus slides was sectioned at 5 µm and air-dried overnight. Staining was performed at Histowiz, Inc. (Brooklyn, NY) using the Leica Bond RX automated stainer (Leica Microsystems). Control samples of normal breast tissue and ductal carcinoma in situ were processed, embedded in paraffin, and sectioned at 4 µm. These slides were dewaxed using xylene and serial dilutions of ethanol. Epitope retrieval was performed by heat-induced epitope retrieval (HIER) of the formalin-fixed, paraffin-embedded tissue using citrate-based pH 6 solution (Leica Microsystems, Cat#AR9961) for 10 min at 95 °C. The tissues were first incubated with peroxide block buffer (Leica Microsystems, Cat# RE7101-CE), followed by incubation with the rabbit heparanase antibody (Novus Biologicals, Cat# NBP303846, RRID: AB_2927437) at 1:500 dilution (this dilution was determined by Histowiz through optimization using HEK 293T cells transfected with a heparanase expression plasmid derived from pcDNA3.1 (RRID: Addgene_79663) using Lipofectamine 3000 (Thermo Fisher Scientific, Cat# L3000015) as positive control for 30 min, followed by DAB rabbit secondary reagents-polymer, DAB refine, and hematoxylin (Bond Polymer Refine Detection Kit, Leica Microsystems, Cat# DS9800)—according to the manufacturer's protocol. The slides were dried, coverslipped (TissueTek-Prisma Coverslipper), and visualized using a Leica Aperio AT2 slide scanner (Leica Microsystems) at 40×. All immunohistochemical staining was carried out at the same time by Histowiz. For the analysis of the tissue microarray (TMA), the Halo TMA module was used to identify the individual TMA cores by constructing a grid over the TMA. All subsequent analysis steps were the same for the slides of ductal carcinoma in situ (DCIS) tissue, normal breast tissue, and the TMA of breast cancers. In the first part of the analysis, the tumor area was identified by training a random forest classifier algorithm to separate viable tumor tissue from any surrounding stroma and necrosis areas. Once the tumor area was identified, the analysis then proceeded to identify positive and negative cells based on heparanase staining within the defined tumor area on each slide and each core from the TMA slide. Positive and negative cells were identified using the Halo Multiplex IHC algorithm

v3.4.1 by first defining the settings for the hematoxylin counterstain, followed by setting thresholds to detect the heparanase stain positivity of weak, moderate, and strong intensities (Halo threshold settings 0.11, 0.35, 0.45). An H-score was then generated following the formula: $(1 \times \% \text{ of cell staining } 1+) + (2 \times \% \text{ cells staining } 2+) + (3 \times \% \text{ cells staining } 3+) = \text{H-score}$ (range 0–300) where weak positive (1+), moderate positive (2+), and strong positive (3+) are defined. For the histology statistical analysis, group differences were determined using Kruskal-Wallis one-way analysis of variance (ANOVA). The comparisons were: different breast cancer sub-types compared to normal and to DCIS, different stages of breast cancer, different grades of breast cancer and % Ki67 expression.

Western blot analysis

Equal numbers of cell types (TNBC MDA-MB 231, Hs 578t, and MDA-MB 468 cells, and nontumorigenic immortal mammary epithelial MCF-10A cells) were seeded and cultured for 48 h to 70–80% confluency. Cell supernatants were collected. Total cell lysates were prepared; protein quantification was performed; and proteins were denatured, separated, and transferred as previously described [9]. For quantitation of heparanase in cell supernatants, 100- μg heparanase, 10- μl cell supernatants, or adjusted volume of cell supernatants (volume inversely proportionate to the total protein mass in the corresponding cell lysate to normalize to cellular mass, with the supernatant sample with the highest corresponding protein mass in lysate set as 10 μl of loaded volume) were loaded onto the 4–20% tris-glycine gels. Unadjusted (with 10 μl supernatant) blots were stained with Ponceau S (Thermo Fisher Scientific) to reveal the loading amount of proteins. The membranes were blocked with 5% nonfat milk at room temperature for an hour and incubated overnight at 4 °C with a primary antibody: heparanase (1:200 dilution; Novus Biologicals, Cat# NBP303846, RRID: AB_2927437) diluted in 5% nonfat milk. The membranes were washed and developed as described previously [9]. Glyceraldehyde-3-phosphate dehydrogenase (GAPDH) (Cell Signaling Technology, Cat #3683, RRID: AB_1642205) or β -actin (Cell Signaling Technology, Cat #3700, RRID: AB_2242334) was used as a loading control. Densitometry was performed on Licor Image Studio (RRID: SCR_015795). The student's t-test was applied to the applicable assays to ascertain significance.

ROC plotter

The ROC Plotter is from microarray data derived from about 36 public datasets of breast cancer patients, and it was used to determine the correlation between heparanase gene expression and chemotherapy response in

TNBC patients via pathological complete response (for non-responders, $n=124$ and for responders, $n=30$) [33].

Verification of heparanase inhibition by OGT 2115 using mobility shift of Syndecan-2

Hs 578t cells were seeded and cultured, and cell lysates were prepared as described in a non-denaturing and non-ionic detergent (1% IGEPAL® CA-630, Sigma, Cat# I3021). OGT 2115 at 20 μM was applied to 100- μg cell lysates in the absence and presence of 50 units of recombinant heparanase enzyme. These treated and untreated lysates were incubated for 6 h at 37 °C. We also grew Hs 578t cells with the vehicle or OGT 2115 for 24 h and then those cells were lysed. Protein samples (100 μg) were loaded onto the 8% tris-glycine gels, transferred, and blocked in 5% nonfat milk for an hour. The membranes were incubated overnight at 4 °C with a syndecan-2 primary antibody (Thermo Fisher Scientific, Cat#36-6200, RRID: AB_2533270) diluted in 5% nonfat milk. Densitometry using β -actin (Genetex, Cat# GTX109639; RRID: AB_1949572) as a loading control was carried out as described above.

Cell viability and eATP assays

TNBC MDA-MB 231, Hs 578t, and MDA-MB 468, and nontumorigenic immortal mammary epithelial MCF-10A cells were plated as previously described and treated with paclitaxel (vehicle), heparan sodium sulfate (50 μM), OGT 2115 (20 μM), A438709 (20 μM), 5-BDBD (20 μM) alone, or different combinations of these drugs. Cells were treated with OGT 2115 and heparan sodium sulfate for 48 h and with paclitaxel, A438709, or 5-BDBD for the final 6 h of the 48-hour time course (we treated cells with paclitaxel for 6 h to replicate exposure times in patients); cell viability was assessed using the PrestoBlue™ HS cell viability reagent (Invitrogen) following the manufacturer's instructions [9]. ATP was assessed in supernatants as described above. Fluorescence readings (excitation and emission ranges: 540–570 nm and 580–610 nm) were evaluated using a Biotech Synergy HT plate reader.

Tumorsphere formation efficiency assay

TNBC MDA-MB 231, Hs 578t, and MDA-MB 468 cell lines were grown and treated with paclitaxel, OGT 2115, and/or heparan sodium sulfate as described above in the “Cell viability and eATP assays” section. Cells were trypsinized, washed, resuspended in 3D Tumorsphere Medium XF (Sigma), and plated at 10 viable cells per well after (45 μM) filtration. Cells were grown for 7 days, and tumorspheres were counted for each different condition using the Etaluma™ Lumascope 620.

Statistical and bioinformatics analyses

When shown to be statistically significant, a post hoc Dunn's test was done to determine p values. P values were adjusted to account for multiple comparisons and an alpha level of 0.05 was used for all tests for IHC analysis. The software GraphPad Prism version 10.0.2 (RRID: SCR_002798) was used for all tests. The student's t-test was applied to the applicable assays to ascertain significance, including for western blot densitometry. One-way ANOVA with Tukey's honestly significant difference (HSD) was calculated to ascertain significance for cell viability, eATP assays and tumorsphere formation efficiency assays.

Bliss independence models were computed from estimated mean viabilities under paclitaxel and OGT 2115 alone via the formula $\text{Log_Viability (Bliss)} = \text{Log_Viability (paclitaxel)} + \text{Log_Viability (OGT 2115)}$. Interaction at each dose was quantified as the ratio of the

predicted viability under the Bliss independence model over the estimated viability under the tested paclitaxel+OGT 2115 combination, with ratios >1 indicating synergy.

Results

Heparanase and heparan sulfate expression in breast cancer

Heparanase expression in breast cancer cell lines and mammary epithelial cells by western blot and ELISAs

To assess the basal expression of heparanase among the cell lines, we performed analysis on TNBC MDA-MB 231, Hs 578t, and MDA-MB 468 cell lines and nontumorigenic immortal epithelial mammary MCF-10A cells, probing for heparanase (Fig. 1; Supplemental Fig. 1). The majority of extracellular heparanase was processed (proteolytically activated; 50 kDa) in all the cell types examined. Unexpectedly, the majority of TNBC cell lines

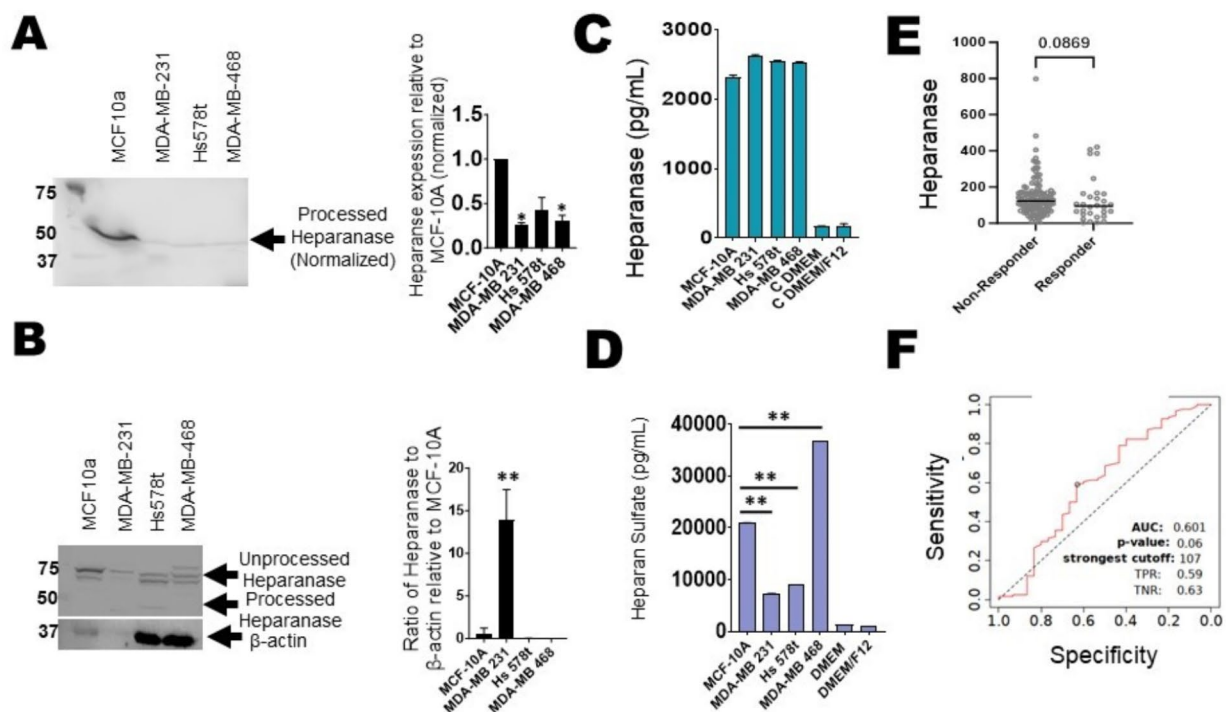


Fig. 1 Heparanase expression in immortal mammary epithelial cells and TNBC cell lines. For the western blot analysis of heparanase, (A) Adjusted volume of cell supernatants, inversely proportionate to the total protein masses in the corresponding cell lysates were probed with heparanase antibody and densitometries analyzed using the student's t-test to determine significance. * represents $p < 0.05$ and ** represents $p < 0.01$ when comparing expression in MCF-10A cells to the expression in TNBC cell lines. (B) Equal amounts of cell lysate from each cell line were probed. Western blots were performed on two biological replicates. The densitometric analyses of the bands were calculated. The student's t-test was performed to determine significance. * represents $p < 0.05$ and ** represents $p < 0.01$ when comparing expression in MCF-10A cells to the expression in TNBC cell lines. (C) Extracellular heparanase expression was determined in nontumorigenic immortal mammary epithelial MCF-10A cells and TNBC MDA-MB 231, Hs 578t, and MDA-MB 468 cells by ELISAs. The standard deviation was calculated from three independent experiments performed in triplicate. The student's t-test was performed with * representing $p < 0.05$ and ** representing $p < 0.01$, comparing expression levels in MCF-10A to those in the TNBC cell lines. (D) Heparan sulfate expression was examined in the supernatants of TNBC cells and control immortal MCF-10A cells via ELISA analysis with MDA-MB 468 expressing the most. The standard deviation was calculated from three independent experiments performed in triplicate. The student's t-test was performed to determine the significance with * representing $p < 0.05$ and ** representing $p < 0.01$ comparing the protein expression in MCF-10A to the protein expressions in the TNBC cell lines. (E) and (F) ROC Plotter was applied to identify whether expression was different between chemotherapy responders ($n = 30$) and non-responders ($n = 124$). Low heparanase expression was not significantly predictive of TNBC patient chemotherapy response (ROC $p = 0.06$, Mann-Whitney $p = 0.087$)

expressed less processed heparanase extracellularly when compared to MCF-10 A cells as assessed by semi-quantitative densitometry. However, a majority of intracellular heparanase expression was unprocessed (molecular weight of 65 kDa). Regarding intracellular processed heparanase, expression was less in the TNBC cell lines compared to MCF-10A cells, with Hs 578t cells expressing the most among the TNBC cell lines. Regarding intracellular unprocessed heparanase, MDA-MB 231 cells expressed the least, while Hs 578t and MDA-MB 468 cells expressed slightly less than MCF-10 A cells. Also, we carried out ELISAs for heparanase expression in the supernatants as an orthogonal method and saw no significant difference between the examined cell types using the appropriate media as a negative control (DMEM for the TNBC cells and DMEM/F12 for MCF-10A) (Fig. 1C).

Heparan sulfate expression by ELISAs in breast cancer cell lines and immortal mammary epithelial cells

TNBC MDA-MB 231, Hs 578t, and MDA-MB 468 cell lines and nontumorigenic immortal epithelial mammary MCF-10A cells were examined for extracellular expression of heparan sulfate via ELISAs (Fig. 1D). Our ELISA results for extracellular heparan sulfate showed that the TNBC MDA-MB 468 cell line expressed significantly more extracellular heparan sulfate than the MCF-10A cell line. In contrast, MCF-10A cells expressed significantly more heparan sulfate than MDA-MB 231 and Hs 578t cells.

Some studies suggest that because heparanase binds to extracellular heparan sulfate, one must account for heparan sulfate levels when interpreting heparanase expression; however, other studies contradict this notion [34]. As some studies suggest that heparanase levels positively correlate with heparan sulfate levels, a more accurate way to analyze heparanase expression may be the ratio of heparanase to heparan sulfate. Hence, a more accurate way to analyze heparanase expression may be by comparing the ratio of heparanase to heparan sulfate. Thus, when heparan sulfate levels are considered, the paradoxically lower expression of heparanase in TNBC cell lines compared to MCF-10A cells may be explained. Our results were based on two biological replicates.

To determine whether heparanase gene expression correlates with chemotherapy response in TNBC patients, we used ROC Plotter to identify whether expression was different between chemotherapy responders and non-responders (Fig. 1E and F). Low heparanase expression was not significantly predictive of TNBC patient chemotherapy response (ROC $p=0.06$, Mann-Whitney $p=0.087$), however the relationship does trend in the direction we would expect per our in vitro results.

We also probed TNBC MDA-MB 231, Hs 578t, and MDA-MB 468 cell lines and nontumorigenic immortal

epithelial mammary MCF-10A cells treated with paclitaxel (100 μM) or ATP (500 μM) for heparanase and saw no significant change in expression for heparanase with chemotherapy or ATP treatment (Supplemental Fig. 2).

Measurement of heparanase expression in human breast cancer samples by immunohistochemistry

A breast cancer tissue array (120 cores specifically with 82 TNBC cores), normal breast tissue slides, and DCIS tissue slides were stained for heparanase expression (Fig. 2A and Supplemental Fig. 3), and statistical analysis was performed (Fig. 2; Supplemental Figs. 4–6). Before tissue array staining, the staining conditions were optimized as described in the methods (Supplemental Fig. 3A). The expression of heparanase was compared among TNBCs ($n=75$), estrogen receptor-positive/progesterone receptor-positive (ER+/PR+) breast cancer ($n=18$), human epidermal growth factor receptor 2-positive (HER2+) breast cancer ($n=14$), normal breast tissue ($n=4$), and DCIS ($n=5$). It is important to note that immunohistochemistry does not differentiate between processed (active) and unprocessed (inactive) heparanase. We found through a one-way ANOVA test that there was no significant difference between breast cancer sub-types in the H-score of heparanase-stained cells. A Kruskal-Wallis test showed that there was no significant difference in the percentages of cells that stained at any level, weakly, moderately or strongly positively for heparanase in tissue sections of normal breast tissue, DCIS, and invasive breast cancers. We also determined through a one-way ANOVA test that there was no significant difference in the H-scores of heparanase-stained cells among TNBC breast cancer stages (IA: $n=9$, IIA: $n=70$, IIB: $n=23$, IIIA: $n=5$, IIIB: $n=8$) (Supplemental Fig. 4). Additionally, a one-way ANOVA test indicated that there was no significant difference in the H-scores of heparanase-stained cells among grades of TNBCs (Grade 1: $n=8$, Grade 2: $n=39$, Grade 3: $n=43$), and a Kruskal-Wallis test comparing cancers with differing % Ki67 expression levels did not find any difference between fraction of heparanase-stained cells or in the H-scores (0%: $n=8$; 1–9%: $n=19$; 10–19%: $n=17$; 20–29%: $n=11$; 30–39%: $n=13$; 40–49%: $n=6$; 50–59%: $n=14$; 60–69%: $n=6$; 70–79%: $n=5$; 80–89%: $n=4$; 90–100%: $n=10$) (Supplemental Figs. 5 and 6).

As previously mentioned, some studies suggest that heparanase binds to cell surface and extracellular matrix heparan sulfate chains, and hence its expression level may positively correlate with heparan sulfate levels; however, this has not been a consistent finding in the literature [34]. Also, given that the expression levels are semi-quantitatively assessed by immunohistochemistry, it is difficult to normalize heparanase to heparan sulfate levels.

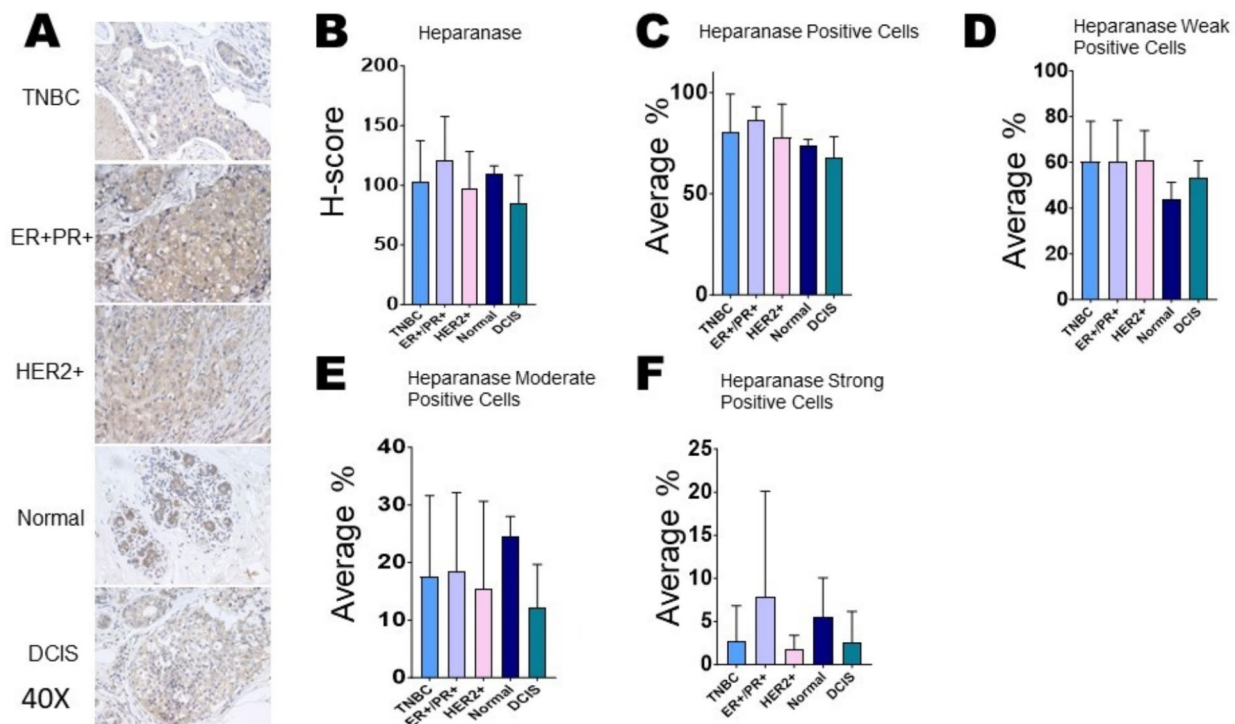


Fig. 2 Statistical analysis for heparanase immunohistochemistry comparing different breast cancer subtypes and normal breast tissue. For the breast cancer tissue array and slides stained for heparanase: TNBC ($n=75$), ER+/PR+ ($n=18$), HER2+ ($n=14$), normal ($n=4$), and DCIS ($n=5$), **(A)** images were taken of heparanase-stained AMSBIO BR1202B breast cancer tissue array and normal and DCIS slides on an Evos FL Auto 2 microscope (40X). **(B)** A one-way ANOVA test indicated no significant difference in the H-scores of heparanase-stained cells among subtypes. A Kruskal-Wallis test indicated that there was no significant difference: **(C)** in the percentage of heparanase positively stained cells in the tissue sections of normal breast tissue, DCIS, and invasive breast cancer subtypes; **(D)** in the percentage of heparanase weakly stained cells in the tissue sections of normal breast tissue, DCIS, and invasive breast cancer subtypes; **(E)** in the percentage of heparanase moderately stained cells in the tissue sections of normal breast tissue, DCIS, and invasive breast cancer subtypes; **(F)** in the percentage of heparanase strongly stained cells in the tissue sections of normal breast tissue, DCIS, and invasive breast cancer subtypes

Effect of heparanase inhibitor on cell viability and eATP

We next combined a heparanase inhibitor (OGT 2115) with chemotherapy (paclitaxel) to assess its impact on the effectiveness of chemotherapy in the TNBC cell lines in comparison to nontumorigenic immortal epithelial mammary MCF-10A cells. For these experiments, all the cell lines were treated with paclitaxel for the final 6 h of a 48-hour time course to simulate the duration of systemic exposure to paclitaxel in patients and with OGT 2115 and heparan sodium sulfate for 48 h (Fig. 3). For this reason, we did not see differences in the loss of viability of cells treated with paclitaxel alone (vehicle addition). Yet, the heparanase inhibitor OGT 2115 (20 μ M) sensitized all three TNBC cell lines—MDA-MB 231, Hs 578t, and MDA-MB 468—to paclitaxel (100 μ M). Additionally, there was further sensitization when heparan sodium sulfate was added to the combination of paclitaxel and OGT 2115. However, there was no sensitization of MCF-10A cells to paclitaxel when concurrently treated with OGT 2115 and heparan sodium sulfate.

Under the same conditions, we also assessed the amount of eATP in the supernatants of

chemotherapy-treated (paclitaxel-treated) cells (Fig. 4). In the presence of OGT 2115 and paclitaxel, we saw significant increases in eATP levels when compared to vehicle addition (paclitaxel alone) in immortal MCF-10A cells and TNBC cell lines. Moreover, there were significant increases in eATP with the addition of heparan sodium sulfate to the combination of paclitaxel and OGT 2115 when compared to the vehicle addition.

We also plotted graphs for the treatments of increasing concentrations of paclitaxel and OGT 2115 (Supplemental Fig. 7). There was some synergy (<0.1 - 1.0) for one dose combination of paclitaxel and OGT 2115 for MDA-MB 231 cells while there were some drug dose combinations that were additive (1 - 1.2) for Hs 578t and MDA-MB 468 cells, using the Bliss independence model for determining synergy.

Thus, the heparanase inhibitor OGT 2115 significantly increased eATP release upon chemotherapy treatment and sensitized TNBCs to chemotherapy.

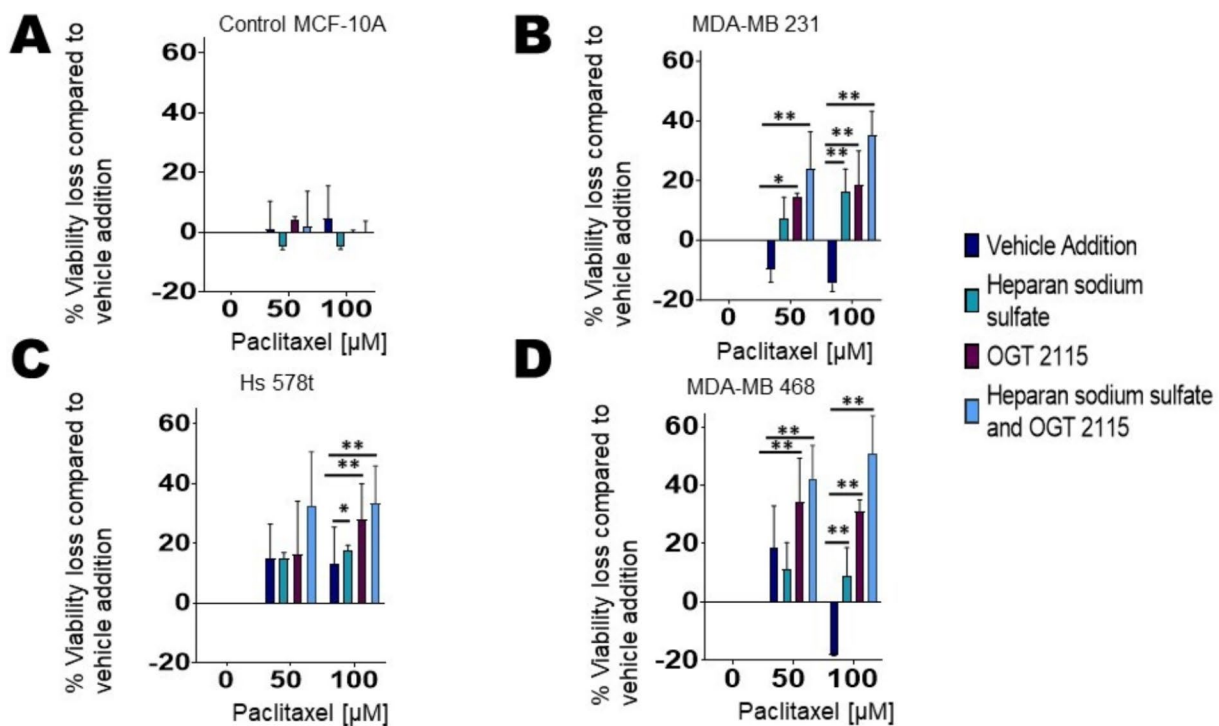


Fig. 3 Effects of heparanase inhibitor OGT 2115 and chemotherapeutic agent paclitaxel on cell viability. Percentage loss of cell viability was measured in treated **(A)** nontumorigenic immortal mammary epithelial MCF-10A cells and TNBC **(B)** MDA-MB 231, **(C)** Hs 578t, and **(D)** MDA-MB 468 cells. The treatments applied were vehicle addition (paclitaxel, purple), heparan sodium sulfate (50 μM, teal), and OGT 2115 (20 μM, purple-red) or the combination (light blue). Heparan sodium sulfate and OGT 2115 were administered for 48 h, and paclitaxel was added for the final 6 h to replicate exposure times in patients. The standard deviation was calculated from three independent experiments performed in triplicate. One-way ANOVA with Tukey's HSD was applied to ascertain significance. * represents $p < 0.05$ and ** represents $p < 0.01$ when comparing vehicle addition to heparan sodium sulfate, OGT 2115, or the combination

Verification that OGT 2115 inhibits heparanase at the concentration utilized

We treated intact Hs 578t cells with OGT 2115 for 24 h before lysing the cells and performing immunoblots on the lysates to analyze expression levels. Hs 578t cells lysed with a non-ionic and non-denaturing detergent were treated with heparanase, heparanase inhibitor OGT 2115, or a combination of both for 6 h; a control (no added heparanase or inhibitor) was also prepared. We focused on the gel mobility of syndecan-2 (a protein known to be physiologically post-translationally modified by heparan sulfate) with a predicted molecular weight of 37 (heparan sulfate modified) and 22 kDa (unmodified protein). Upon immunoblotting, lysates of vehicle or OGT 2115-treated intact cells, we observed an increase in the intensity of both the 37 and 22 kDa molecular weight bands in the OGT 2115-treated cells (Supplemental Fig. 8). This is consistent with degradation of syndecans upon loss of heparan sulfate chains due to exposure of protease cleavable sites of the core protein by endogenously expressed heparanase, as has previously been described [35–38]. Furthermore, when cells were lysed with non-denaturing and non-ionic detergents and were treated with heparanase, we then again observed

loss of both 37 and 22 kDa bands. This effect was partially reversed by concurrently treating the lysates with OGT 2115. This data shows that OGT 2115 inhibits heparanase at the concentrations used for the experiments.

Role of purinergic signaling in enhancing chemotherapy-induced TNBC cell death with the application of heparanase inhibitors

We had previously demonstrated that eATP exerts cytotoxic effects on TNBC cells through P2RX4 and P2RX7 receptors [9]. We sought to verify whether the sensitization of TNBC cells to paclitaxel by OGT 2115 is dependent on eATP-induced activation of P2RX4 or P2RX7 (Fig. 5). We chose Hs 578t cells for this experiment because we detected the largest increase in eATP and percentage loss of cell viability when this cell line was exposed to the combination of paclitaxel, OGT 2115, and heparan sodium sulfate. We did observe a significant reversal of the sensitizing effects of OGT 2115 on cell viability and eATP release when experimenting in the presence of the P2RX7 inhibitor A438079 (Fig. 5A and C) or the P2RX4 inhibitor 5-BDBD (Fig. 5B and D). This was revealed by a significant decrease in eATP ($p < 0.0001$) and increased cell viability ($p < 0.0001$) when comparing

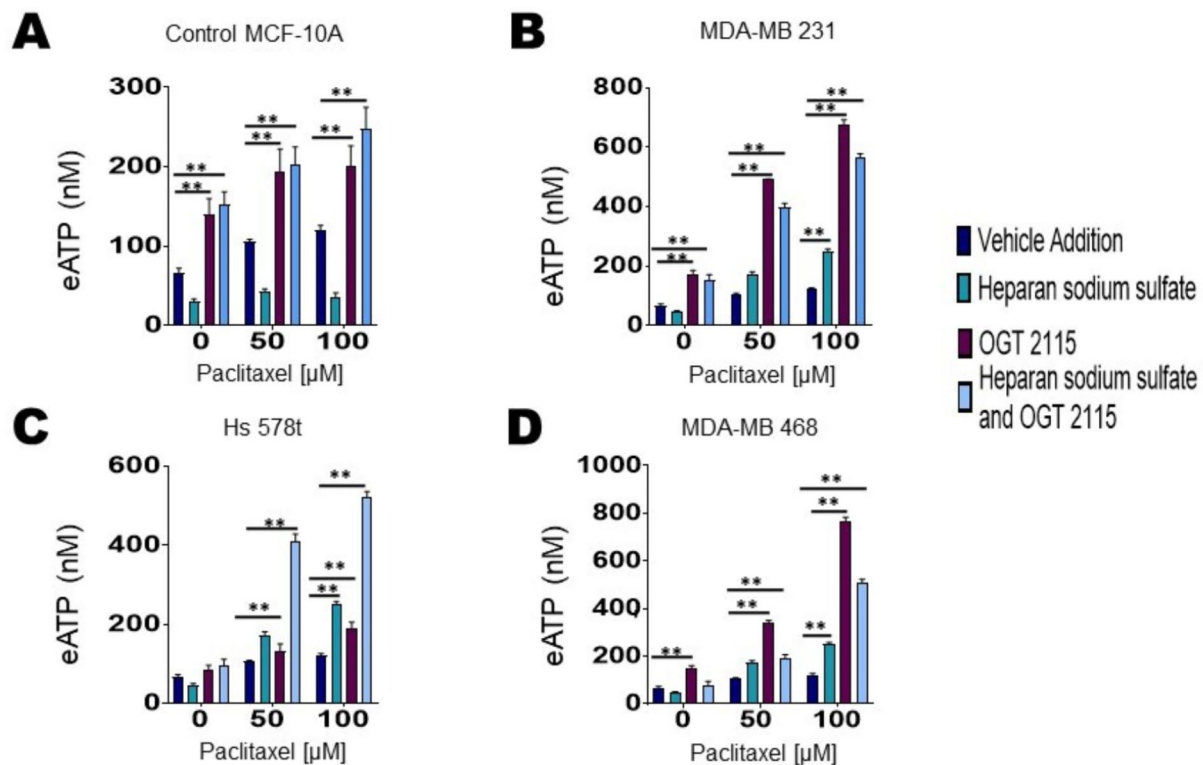


Fig. 4 Heparanase inhibitor OGT 2115 and chemotherapeutic agent paclitaxel influence extracellular ATP concentrations. Extracellular ATP concentrations were measured in the supernatants of treated (A) nontumorigenic immortal mammary epithelial MCF-10 A cells and TNBC (B) MDA-MB 231, (C) Hs 578t, and (D) MDA-MB 468 cells. The treatments: vehicle addition (paclitaxel, purple), heparan sodium sulfate (50 μM, teal), and OGT 2115 (20 μM, purple-red), or the combination regimen (light blue). Heparan sodium sulfate and OGT 2115 were administered for 48 h and paclitaxel was added for the final 6 h to replicate exposure times in patients. The standard deviation was calculated from three independent experiments performed in triplicate. One-way ANOVA with Tukey's HSD was applied to ascertain significance. * represents $p < 0.05$ and ** represents $p < 0.01$ when comparing vehicle addition to heparan sodium sulfate, OGT 2115, or the combination regimen

the combination of paclitaxel with OGT 2115 to that of paclitaxel with OGT 2115 and A438709. We observed a significant decrease in eATP ($p < 0.0001$) and increased cell viability ($p < 0.0001$) when comparing the combination of paclitaxel, heparan sodium sulfate, and OGT 2115 to paclitaxel, heparan sodium sulfate, OGT 2115, and 5-BDBD. Hence, the P2RX7 blocker A438709 and the P2RX4 blocker 5-BDBD reversed the capacity of OGT 2115, and that of heparan sulfate combined with OGT 2115, to sensitize cells to and augment eATP release induced by paclitaxel treatment of TNBC cell lines.

This data demonstrates that the exaggerated loss of cell viability observed when OGT 2115 and heparan sulfate are combined with paclitaxel is dependent on the activation of both P2RX4 and P2RX7 by eATP.

Impact of purinergic signaling on cancer-initiating cells

We then analyzed the effects of purinergic signaling on cancer-initiating cells by carrying out tumorsphere formation efficiency assays. TNBC cell lines were treated with paclitaxel, OGT 2115, and/or heparan sodium sulfate and then passed through cell strainers and plated

and maintained as spheroids as described in the methods. After 7 days, we measured the fraction of wells that had been plated with at least one viable cell that showed tumorsphere formation. We noted that tumorsphere formation efficiency was decreased for all TNBC cells - MDA-MB 231, MDA-MB 468, and Hs 578t - in the presence of paclitaxel, heparan sodium sulfate, and OGT 2115 (Fig. 6) compared to vehicle treatment and paclitaxel alone. Hence, this data suggests that the heparanase inhibitor OGT 2115 suppresses the cancer-initiating cell fraction.

Discussion

Chemotherapy is still the standard treatment for TNBC. A major drawback of chemotherapy is its inability to eliminate macroscopic metastatic disease, despite transient responses. Therapeutic approaches that increase the magnitude of responses and expand those responses to otherwise chemotherapy-insensitive tumors are urgently needed. Extracellular ATP, in the high micromolar to millimolar range, has been demonstrated to be cytotoxic to cancer cell lines. We have demonstrated that

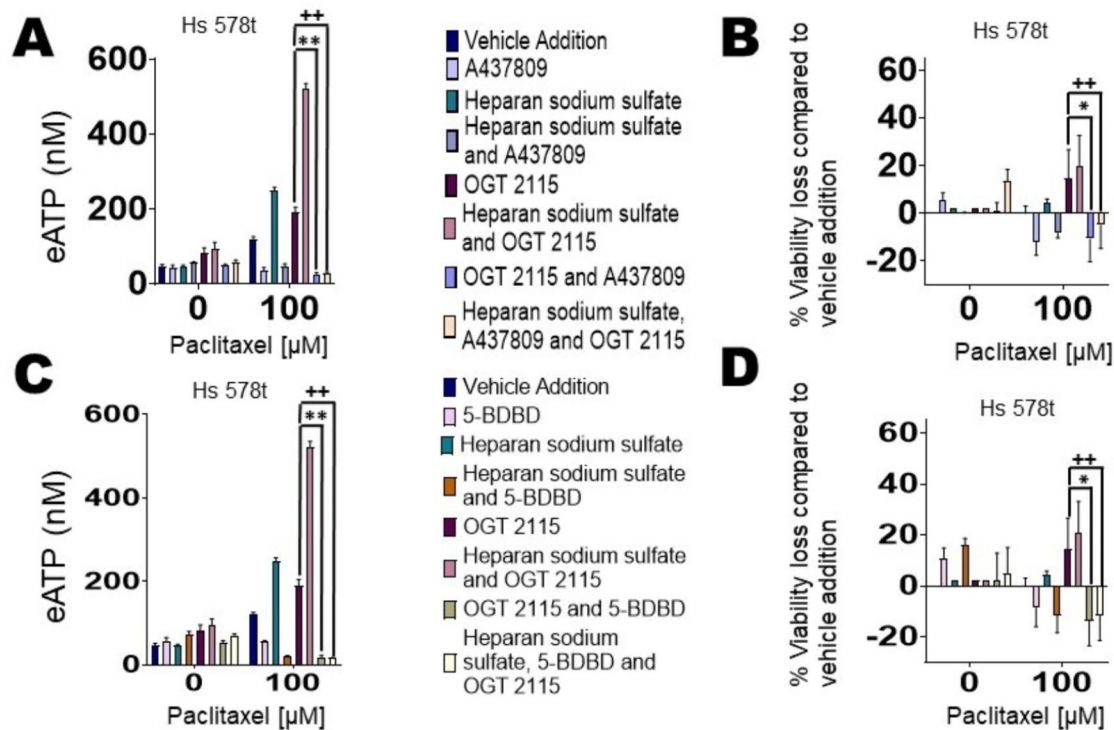


Fig. 5 Reversal of heparanase inhibitor's effects by P2RX4 and P2RX7 inhibitors. For **(A)** and **(B)**, Hs 578t cells were treated with OGT 2115 (20 μM, 48 h), paclitaxel (100 μM, the final 6 h of the 48-hour time course to replicate exposure times in patients), heparan sodium sulfate (50 μM, 48 h), A437809 (20 μM, 6 h), or a combination of the different drug agents. The standard deviation was calculated from three independent experiments performed in triplicate. One-way ANOVA with Tukey's HSD was applied to ascertain significance. * represents $p < 0.05$ and ** represents $p < 0.01$ when comparing paclitaxel and OGT 2115 to paclitaxel, OGT 2115 and A437809 and ++ represents $p < 0.01$ when comparing paclitaxel, OGT 2115 and heparan sulfate to paclitaxel, OGT 2115, heparan sodium sulfate and A437809. For **(C)** and **(D)** Hs 578t cells were treated with OGT 2115 (20 μM, 48 h), paclitaxel (100 μM, final 6 h of the 48-hour time course to replicate exposure times in patients), heparan sodium sulfate (50 μM, 48 h), 5-BDBD (20 μM, 6 h), or combinations. The standard deviation was calculated from three independent experiments performed in triplicate. One-way ANOVA with Tukey's HSD was applied to ascertain significance. * represents $p < 0.05$; ** represents $p < 0.01$ when comparing paclitaxel and OGT 2115 to paclitaxel, OGT 2115 and 5-BDBD and ++ represents $p < 0.01$ when comparing paclitaxel, OGT 2115 and heparan sulfate to paclitaxel, OGT 2115, heparan sodium sulfate and 5-BDBD

chemotherapy treatment increases eATP release from TNBC cells [9]. We also showed that ecto-ATPase inhibitors enhance chemotherapy-induced eATP release from TNBC cells and augment chemotherapy-induced cell death [9]. However, this strategy is limited by the presence of multiple families of ecto-ATPases in humans, each with multiple members, thus complicating the design of synthetic inhibitors. Hence, a broad-spectrum ectoATPase inhibitor is required.

Heparan sulfate has previously been shown to modulate the proliferation and survival of cancer cells by many mechanisms. The "S" domains of heparan sulfate are regions in which 2 N sulfated glucosamine residues occur in contiguous sequences, in contrast to other regions such as the "NA/NS" or transition domains where N-acetylated glucosamine alternates with N-sulfated glucosamine [39]. It is the disaccharide sequence 2-O sulfated Iduronic acid-2 N, 6-O sulfated glucosamine in the "S" domains of heparan sulfate that acts as selective docking sites for proteins [39]. Heparan sulfate has been shown to bind to multiple proteins that are relevant

to proliferation, growth, migration, and immunity. These include morphogens such as hedgehog, decapentaplegic, and wingless [40, 41]. Another key activity of heparan sulfate may be related to the modulation of angiogenesis through VEGF signaling [35]. In addition, PDGFR α signaling is upregulated by sulfatase 2, which removes 6-O sulfates from heparan sulfate [42]. Hence, heparan sulfate may affect cancer cells by modulating signaling by multiple different ligands.

In addition, polysulfated polysaccharides have been revealed to inhibit multiple classes of ecto-ATPases, thus attenuating the degradation of ATP [11, 12]. Therefore, we hypothesized that increasing heparan sulfate in the microenvironment of triple-negative cancer cells using heparanase inhibitors would enhance eATP concentrations in the pericellular environment of chemotherapy-treated TNBC cells and augment chemotherapy-induced cell death.

Unexpectedly, our immunoblot results revealed that heparanase is highly expressed intracellularly and extracellularly in immortal mammary epithelial cells

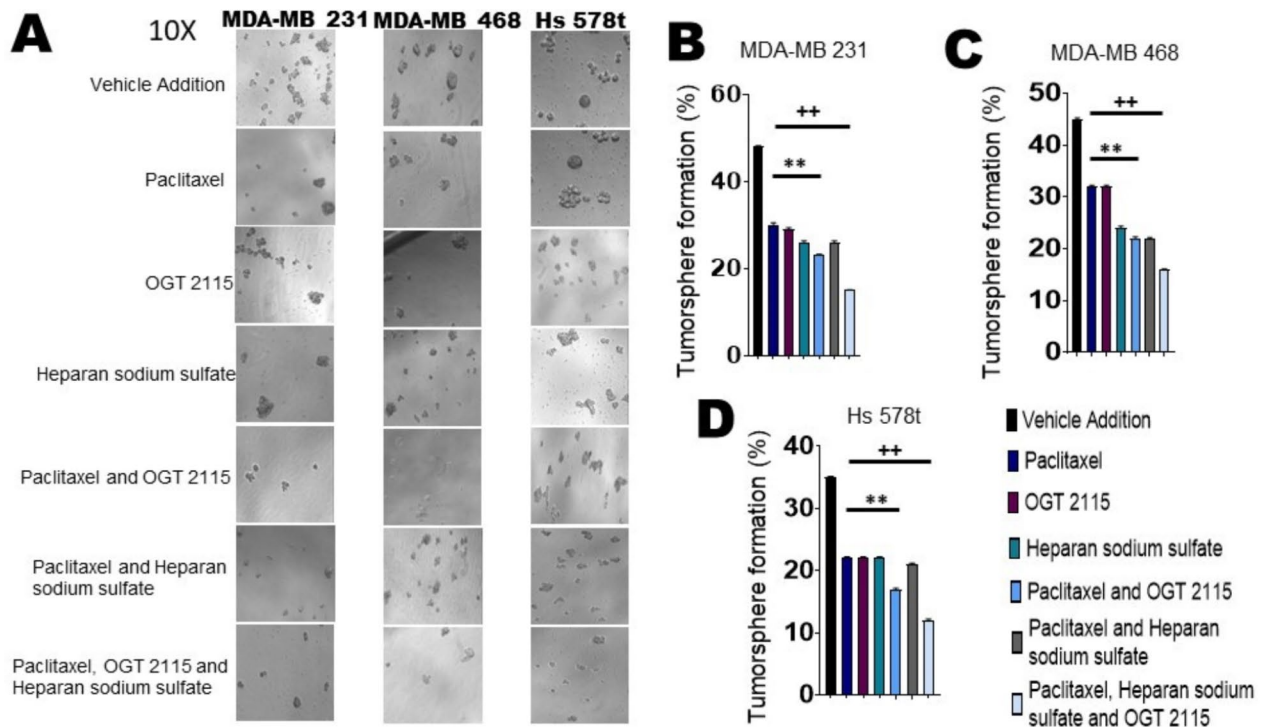


Fig. 6 Tumorsphere formation efficiency assays for treated TNBC cells. Effects of heparanase inhibitor on cancer-initiating cells were determined through the tumorsphere formation efficiency assay in which TNBC cell lines were treated with vehicle (DMSO), paclitaxel (100 μ M, final 6 h of the 48-hour time course to replicate exposure times in patients), heparan sodium sulfate (50 μ M, 48 h), OGT 2115 (20 μ M, 48 h), or the different combinations listed. **(A)** Tumorsphere images obtained (10 \times) are displayed for each treatment of MDA-MB 231, MDA-MB 468, and Hs 578t cells with paclitaxel, OGT 2115, heparan sodium sulfate, or the different combinations. The combination regimens showed a significant decrease in tumorsphere formation when compared to the single-agent treatments of vehicle, paclitaxel, heparan sodium sulfate, or OGT 2115 treated **(B)** MDA-MB 231, **(C)** MDA-MB 468, and **(D)** Hs 578t cells. Three independent experiments were performed in triplicate. One-way ANOVA with Tukey's HSD was applied to ascertain significance. ** represents $p < 0.01$ when comparing paclitaxel to paclitaxel and OGT 2115. ++ represents $p < 0.01$ when comparing paclitaxel to paclitaxel, heparan sodium sulfate, and OGT 2115

when compared to TNBC cells. Also paradoxically, the ELISA and immunohistochemistry results did not show increased heparanase expression levels in TNBC cell lines or invasive breast cancers as compared to immortal mammary epithelial cells or normal breast tissue and DCIS, respectively. As noted in the results, this could be due to the dependence of expression levels of heparanase on binding to heparan sulfate and its transcriptional induction by heparan sulfate [34, 43]. Hence, the ratio of heparanase to heparan sulfate expression may be a better measure of heparanase activity.

As heparan sulfate inhibits multiple classes of ecto-ATPases, we sought to determine if heparanase inhibitors, which inhibit heparan sulfate degradation, can augment chemotherapy-induced cytotoxicity and exacerbate chemotherapy-induced eATP release [11, 12]. We showed that the combination of the heparanase inhibitor OGT 2115 with chemotherapy (paclitaxel) increased eATP concentrations and sensitized TNBCs to chemotherapy. Additionally, specific inhibitors of P2RX4 and P2RX7 eATP receptors caused eATP levels and TNBC cell death to return to basal levels after exposure to the

heparanase inhibitor, confirming that these effects are dependent on these purinergic receptors; we have demonstrated before that these receptors are necessary for chemotherapy-induced eATP release from TNBC cells and for the sensitization of TNBC cells to paclitaxel by ectoATPase inhibitors [9].

Additionally, we evaluated the effects of combinations of heparanase inhibitors and chemotherapy on cancer-initiating cells, as failure to eradicate these cells results in the capacity of cytotoxic chemotherapy alone to eliminate metastatic TNBC [44–47]. We showed that in the presence of chemotherapy combined with the heparanase inhibitor, there were fewer surviving cancer-initiating cells, as assessed by tumorsphere efficiency assay, across all TNBC cell lines.

eATP is a known immune danger signal, and its metabolite adenosine is considered a potent immunosuppressant; hence, additional research is needed to assess the immune effects of ecto-ATPase inhibition by heparan sulfate using immunocompetent in vivo models of TNBC. Additionally, more work is needed to assess whether the chemosensitizing effect on TNBC

cells occurs through nonspecific permeabilization of cell membranes by P2RX7 macropore formation or whether additional downstream pathways such as pyroptosis are involved. We will focus our future research on clarifying these questions.

Conclusion

Heparanase inhibition sensitizes TNBC cell lines to chemotherapy by increasing eATP concentrations in the microenvironment of chemotherapy-treated cells. Hence, heparanase inhibitors may generate deeper and more durable responses in combination with chemotherapy. A major focus of our future goals would be to confirm these hypotheses *in vivo*. As eATP is a noted immune danger signal, it will also be critical to establish the immune effects of this therapeutic strategy and implications for combination with current immunotherapeutic strategies.

Abbreviations

ALDH	Aldehyde dehydrogenase
ANOVA	Analysis of variance
AMP	Adenosine monophosphate
APC	Allophycocyanine
ATP	Adenosine triphosphate
BSA	Bovine serum albumin
CM	Complete medium
DCIS	Ductal carcinoma in situ
DMSO	Dimethyl sulfoxide
eATP	Extracellular adenosine triphosphate
ECM	Extracellular matrix
ELISA	Enzyme-linked immunoassay
E-NPPase	Ecto-nucleotide pyrophosphatases/phosphodiesterases
ENTPD1	Ecto-nucleoside triphosphate diphosphohydrolases 1
EGF	Epidermal growth factor
ER+	Estrogen receptor-positive
EXT1	Exostosin glycosyltransferase 1
EXT2	Exostosin glycosyltransferase 2
FGFs	Fibroblast growth factors
FITC	Fluorescein isothiocyanate
5'-NTs	5' nucleotidases
GAPDH	Glyceraldehyde-3-phosphate dehydrogenase
HIER	Heat-induced epitope retrieval
HER2+	Human epidermal growth factor receptor 2-positive
HS	Heparan sulfate
HSD	Honestly significant difference
MFI	Mean fluorescence intensity
mM	Millimolar
nM	Nanomolar
O/E	Overexpression
PBS	Phosphate-buffered saline
PR+	Progesterone receptor-positive
PE	Phycoerythrin
TMA	Tissue microarray
TNAP	Tissue nonspecific alkaline phosphatases
TNBC	Triple-negative breast cancer
µg	Microgram
µL	Microliter
µm	Micrometer
µM	Micromolar
VEGFs	Vascular endothelial growth factors

Supplementary Information

The online version contains supplementary material available at <https://doi.org/10.1186/s13058-024-01906-6>.

Supplementary Material 1
Supplementary Material 2
Supplementary Material 3
Supplementary Material 4
Supplementary Material 5
Supplementary Material 6
Supplementary Material 7
Supplementary Material 8
Supplementary Material 9
Supplementary Material 10
Supplementary Material 11
Supplementary Material 12
Supplementary Material 13
Supplementary Material 14

Acknowledgements

The authors would like to thank scientific editor Angela Dahlberg, Division of Medical Oncology, The Ohio State University Comprehensive Cancer Center, for editing this manuscript.

Author contributions

All authors contributed to the review and analysis. JMM performed a majority of the assays with JD carrying out the Western blot analyses, and LMM carrying out the immunohistochemistry analysis. JJR carried out the ROC plotter analysis. PMS carried out tests for synergistic effects of OGT 2115 and paclitaxel. JMM and MAC conceived of and designed the experiments, reviewed the data, and authored and edited the manuscript.

Funding

Research reported in this publication was supported by The Ohio State University Comprehensive Cancer Center and supported by NCI/NIH (P30CA016058). This publication was also supported in part by the National Center for Advancing Translational Sciences of the National Institutes of Health (KL2TR002734). Institutions that provided funding support had no role in the design or conduct of this study or the preparation of the manuscript. The content is solely the responsibility of the authors and does not necessarily represent the official views of the National Institutes of Health.

Data availability

No datasets were generated or analysed during the current study.

Declarations

Ethics approval and consent to participate

Not applicable.

Consent for publication

Not applicable.

Competing interests

The authors declare no competing interests.

Author details

¹Division of Medical Oncology, The Ohio State University Comprehensive Cancer Center, 410 W 10th Ave., Columbus, OH 43210, USA

²Department of Radiation Oncology, The Ohio State University Comprehensive Cancer Center, 410 W 10th Ave., Columbus, OH 43210, USA

³Division of Hematology, The Ohio State University Comprehensive Cancer Center, 410 W 10th Ave., Columbus, OH 43210, USA

⁴Division of Cancer Prevention and Control, Department of Internal Medicine, The Ohio State University, Suite 525, 1590 North High St., Columbus, OH 43201, USA

⁵Division of Biostatistics, The Ohio State University College of Public Health, 1841 Neil Ave., Columbus, OH 43210, USA

⁶Division of Medical Oncology, 460 W 12th Ave., 888 BRT, Columbus, OH 43210, USA

Received: 17 April 2024 / Accepted: 17 October 2024

Published online: 06 November 2024

References

1. Breast, Cancer. [<https://www.who.int/cancer/prevention/diagnosis-screening/breast-cancer/en/>]
2. Dent R, Hanna WM, Trudeau M, Rawlinson E, Sun P, Narod SA. Pattern of metastatic spread in triple-negative breast cancer. *Breast Cancer Res Treat.* 2009;115(2):423–8.
3. Fisher CS, Ma CX, Gillanders WE, Aft RL, Eberlein TJ, Gao F, Margenthaler JA. Neoadjuvant chemotherapy is associated with improved survival compared with adjuvant chemotherapy in patients with triple-negative breast cancer only after complete pathologic response. *Ann Surg Oncol.* 2012;19(1):253–8.
4. Ovcaricek T, Frkovic SG, Matos E, Mozina B, Borstnar S. Triple negative breast cancer - prognostic factors and survival. *Radiol Oncol.* 2011;45(1):46–52.
5. Bakker WW, Donker RB, Timmer A, van Pampus MG, van Son WJ, Aar-noudse JG, van Goor H, Niezen-Koning KE, Navis G, Borghuis T, et al. Plasma hemopexin activity in pregnancy and preeclampsia. *Hypertens Pregnancy.* 2007;26(2):227–39.
6. Pellegatti P, Raffaghello L, Bianchi G, Piccardi F, Pistoia V, Di Virgilio F. Increased level of extracellular ATP at tumor sites: in vivo imaging with plasma membrane luciferase. *PLoS ONE.* 2008;3(7):e2599.
7. Yegutkin GG. Nucleotide- and nucleoside-converting ectoenzymes: important modulators of purinergic signalling cascade. *Biochim Biophys Acta.* 2008;1783(5):673–94.
8. Fan M, Yan PS, Hartman-Frey C, Chen L, Paik H, Oyer SL, Salisbury JD, Cheng AS, Li L, Abbosh PH, et al. Diverse gene expression and DNA methylation profiles correlate with differential adaptation of breast cancer cells to the antiestrogens tamoxifen and fulvestrant. *Cancer Res.* 2006;66(24):11954–66.
9. Manouchehri JM, Datta J, Willingham N, Wesolowski R, Stover D, Ganju RK, Carson WE, Ramaswamy B, Cherian MA. Augmentation of Extracellular ATP Synergizes with Chemotherapy in Triple negative breast Cancer. *Front Oncol.* 2022;12:855032.
10. Zimmermann H, Zebisch M, Strater N. Cellular function and molecular structure of ecto-nucleotidases. *Purinergic Signal.* 2012;8(3):437–502.
11. Lopez V, Schäkel L, Schuh HJM, Schmidt MS, Mirza S, Renn C, Pelletier J, Lee SY, Sévigny J, Alban S et al. Sulfated Polysaccharides from Macroalgae are potent dual inhibitors of human ATP-Hydrolyzing ectonucleotidases NPP1 and CD39. *Mar Drugs* 2021, 19(2).
12. Vieira JBTR VP, Stefanello D, Balz FM, Morsch VM. Schetinger: heparin and chondroitin sulfate inhibit adenine nucleotide hydrolysis in liver and kidney membrane enriched fractions. *Int J Biochem Cell Biol.* 2001;33:1193–201.
13. Knelson EH, Nee JC, Blobe GC. Heparan sulfate signaling in cancer. *Trends Biochem Sci.* 2014;39(6):277–88.
14. Gomes AM, Stelling MP, Pavao MS. Heparan sulfate and heparanase as modulators of breast cancer progression. *Biomed Res Int.* 2013;2013:852093.
15. Pisano C, Vlodavsky I, Ilan N, Zunino F. The potential of heparanase as a therapeutic target in cancer. *Biochem Pharmacol.* 2014;89(1):12–9.
16. Lanzi C, Cassinelli G. Heparan Sulfate mimetics in Cancer Therapy: the challenge to define structural determinants and the relevance of targets for optimal activity. *Molecules* 2018, 23(11).
17. Vlodavsky I, Beckhove P, Lerner I, Pisano C, Meirovitz A, Ilan N, Elkin M. Significance of heparanase in cancer and inflammation. *Cancer Microenviron.* 2012;5(2):115–32.
18. Hassan N, Greve B, Espinoza-Sanchez NA, Gotte M. Cell-surface heparan sulfate proteoglycans as multifunctional integrators of signaling in cancer. *Cell Signal.* 2021;77:109822.
19. Ota H, Sato H, Mizumoto S, Wakai K, Yoneda K, Yamamoto K, Nakanishi H, Ikeda J-I, Sakamoto S, Ichikawa T, et al. Switching mechanism from AR to EGFR signaling via 3-O-sulfated heparan sulfate in castration-resistant prostate cancer. *Sci Rep.* 2023;13(1):11618.
20. Cross MJC-WL. FGF and VEGF function in angiogenesis signalling pathways, biological responses and therapeutic inhibition. *Trends Pharmacol Sci.* 2001;22(4):201–7.
21. Vlodavsky I, Elkin M, Abboud-Jarrou G, Levi-Adam F, Fuks L, Shafat I, Ilan N. Heparanase: one molecule with multiple functions in cancer progression. *Connect Tissue Res.* 2008;49(3):207–10.
22. Schubert SY, Ilan N, Shushy M, Ben-Izhak O, Vlodavsky I, Goldshmidt O. Human heparanase nuclear localization and enzymatic activity. *Lab Invest.* 2004;84(5):535–44.
23. Ramani VC, Vlodavsky I, Ng M, Zhang Y, Barbieri P, Noseda A, Sanderson RD. Chemotherapy induces expression and release of heparanase leading to changes associated with an aggressive tumor phenotype. *Matrix Biol.* 2016;55:22–34.
24. Shteingauz A, Boyango I, Naroditsky I, Hammond E, Gruber M, Doweck I, Ilan N, Vlodavsky I. Heparanase enhances Tumor Growth and Chemoresistance by promoting Autophagy. *Cancer Res.* 2015;75(18):3946–57.
25. Ikuta M, Manrayama KAPK, Enomoto S, Yanagishita M. Expression of heparanase in oral cancer cell lines and oral cancer tissues. *Oral Oncol* 2001(37):177–84.
26. Vlodavsky I, Elkin M, Ilan N. Impact of heparanase and the tumor microenvironment on cancer metastasis and angiogenesis: basic aspects and clinical applications. *Rambam Maimonides Med J.* 2011;2(1):e0019.
27. Li X, Xu SJ, Jin B, Lu HS, Zhao SK, Ding XF, Xu LL, Li HJ, Liu SC, Chen J, et al. Heparanase inhibitor OGT 2115 induces prostate cancer cell apoptosis via the downregulation of MCL-1. *Oncol Lett.* 2024;27(2):83.
28. Agelidis AM, Hadigal SR, Jaishankar D, Shukla D. Viral activation of Heparanase drives pathogenesis of herpes simplex Virus-1. *Cell Rep.* 2017;20(2):439–50.
29. du Bois A, Luck HJ, Meier W, Adams HP, Mobus V, Costa S, Bauknecht T, Richter B, Warm M, Schroder W, et al. A randomized clinical trial of cisplatin/paclitaxel versus carboplatin/paclitaxel as first-line treatment of ovarian cancer. *J Natl Cancer Inst.* 2003;95(17):1320–9.
30. Fleck D, Mundt N, Bruentgens F, Geilenkirchen P, Machado PA, Veitinger T, Veitinger S, Lipartowski SM, Engelhardt CH, Oldiges M, et al. Distinct purinergic signaling pathways in prepubescent mouse spermatogonia. *J Gen Physiol.* 2016;148(3):253–71.
31. Balazs B, Danko T, Kovacs G, Koles L, Hediger MA, Zsembery A. Investigation of the inhibitory effects of the benzodiazepine derivative, 5-BDBD on P2X4 purinergic receptors by two complementary methods. *Cell Physiol Biochem.* 2013;32(1):11–24.
32. Bat-Erdene U, Quan E, Chan K, Lee BM, Matook W, Lee KY, Rosales JL. Neutrophil TLR4 and PKR are targets of breast cancer cell glycosaminoglycans and effectors of glycosaminoglycan-induced APRIL secretion. *Oncogenesis.* 2018;7(6):45.
33. Fekete JT, Gyorffy B. ROCplot.org: validating predictive biomarkers of chemotherapy/hormonal therapy/anti-HER2 therapy using transcriptomic data of 3,104 breast cancer patients. *Int J Cancer.* 2019;145(11):3140–51.
34. Marchetti D, Liu S, Spohn WC, Carson DD. Heparanase and a synthetic peptide of heparan sulfate-interacting protein recognize common sites on cell surface and extracellular matrix heparan sulfate. *J Biol Chem.* 1997;272(25):15891–7.
35. Purushothaman A, Uyama T, Kobayashi F, Yamada S, Sugahara K, Rapraeger AC, Sanderson RD. Heparanase-enhanced shedding of syndecan-1 by myeloma cells promotes endothelial invasion and angiogenesis. *Blood.* 2010;115(12):2449–57.
36. Jung O, Trapp-Stamborski V, Purushothaman A, Jin H, Wang H, Sanderson RD, Rapraeger AC. Heparanase-induced shedding of syndecan-1/CD138 in myeloma and endothelial cells activates VEGFR2 and an invasive phenotype: prevention by novel synstatins. *Oncogenesis.* 2016;5(2):e202–202.
37. Sharma P, Kapoor D, Shukla D. Role of Heparanase and Syndecan-1 in HSV-1 release from infected cells. *Viruses* 2022, 14(10).
38. De Rossi G, Evans AR, Kay E, Woodfin A, McKay TR, Nourshargh S, Whiteford JR. Shed syndecan-2 inhibits angiogenesis. *J Cell Sci.* 2014;127(21):4788–99.
39. Viviano BL, Paine-Saunders S, Gasiunas N, Gallagher J, Saunders S. Domain-specific modification of Heparan Sulfate by Oslu1 modulates the binding of the bone morphogenetic protein antagonist Noggin*. *J Biol Chem.* 2004;279(7):5604–11.
40. Baeg GH, Lin X, Khare N, Baumgartner S, Perrimon N. Heparan sulfate proteoglycans are critical for the organization of the extracellular distribution of Wingless. *Development.* 2001;128(1):87–94.
41. Takei Y, Ozawa Y, Sato M, Watanabe A, Tabata T. Three *Drosophila* EXT genes shape morphogen gradients through synthesis of heparan sulfate proteoglycans. *Development.* 2004;131(1):73–82.

42. Phillips JJ, Huillard E, Robinson AE, Ward A, Lum DH, Polley MY, Rosen SD, Rowitch DH, Werb Z. Heparan sulfate sulfatase SULF2 regulates PDGFR α signaling and growth in human and mouse malignant glioma. *J Clin Investig*. 2012;122(3):911–22.
43. Gingis-Velitski S, Zetser A, Kaplan V, Ben-Zaken O, Cohen E, Levy-Adam F, Bashenko Y, Flugelman MY, Vlodavsky I, Ilan N. Heparanase uptake is mediated by cell membrane heparan sulfate proteoglycans. *J Biol Chem*. 2004;279(42):44084–92.
44. Clark DW, Palle K. Aldehyde dehydrogenases in cancer stem cells: potential as therapeutic targets. *Ann Transl Med*. 2016;4(24):518.
45. Januchowski R, Wojtowicz K, Sterzyńska K, Sosifńska P, Andrzejewska M, Zawierucha P, Nowicki M, Zabel M. Inhibition of ALDH1A1 activity decreases expression of drug transporters and reduces chemotherapy resistance in ovarian cancer cell lines. *Int J Biochem Cell Biol*. 2016;78:248–59.
46. Januchowski R, Wojtowicz K, Zabel M. The role of aldehyde dehydrogenase (ALDH) in cancer drug resistance. *Biomed Pharmacother*. 2013;67(7):669–80.
47. Mérida I, Torres-Ayuso P, Ávila-Flores A, Arranz-Nicolás J, Andrada E, Tello-Lafoz M, Liébana R, Arcos R. Diacylglycerol kinases in cancer. *Adv Biol Regul*. 2017;63:22–31.

Publisher's note

Springer Nature remains neutral with regard to jurisdictional claims in published maps and institutional affiliations.